Graphical Abstract

An Augmented Reality-enabled Digital Twin System for Reconfigurable Soft Robots: Visualization, Simulation and Interaction

Zhongyuan Liao, Wanzhen Wei, Leihan Zhang, Yuer Gao, Yi Cai

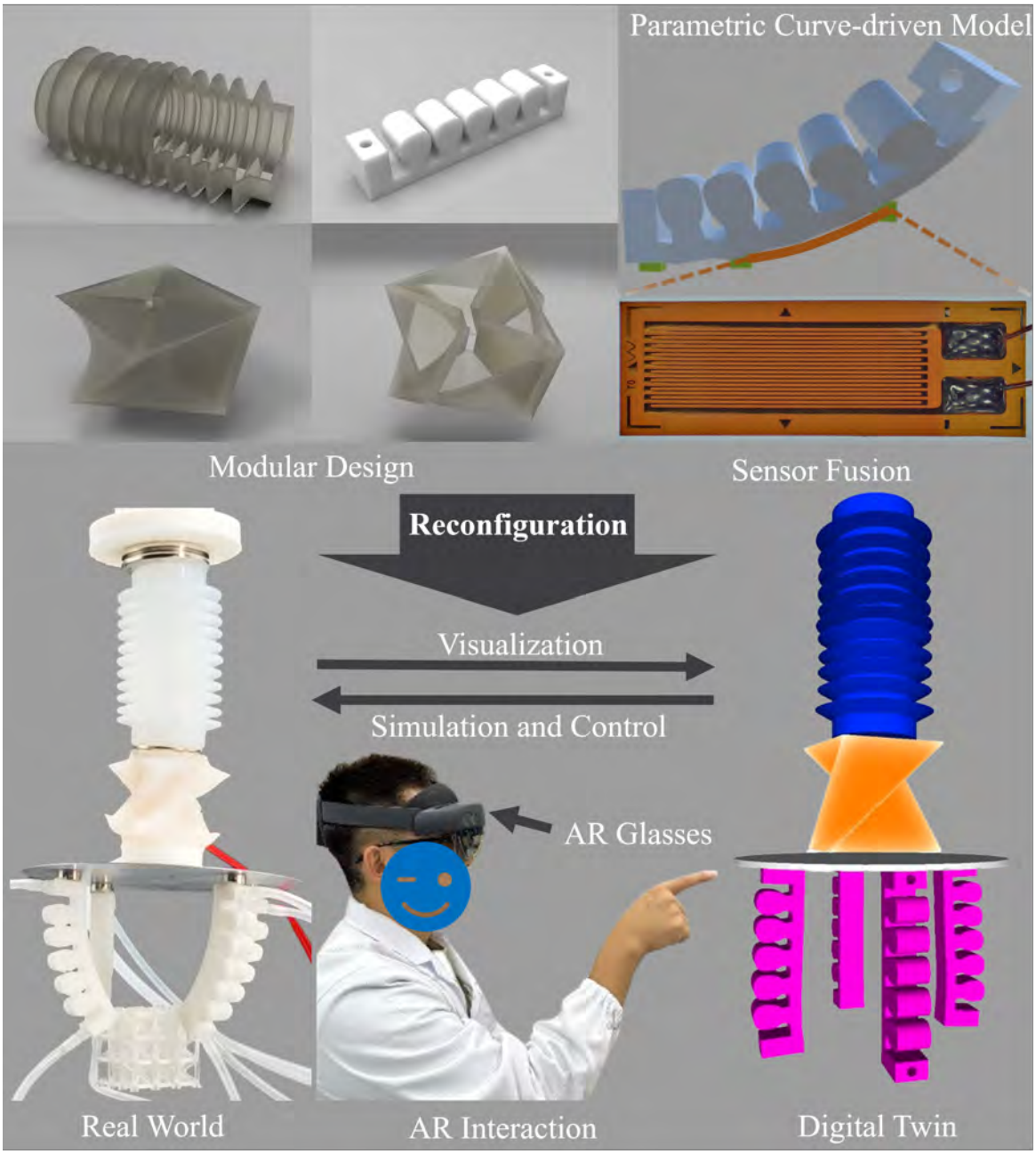

Email address: yicai@hkust-gz.edu.cn (Yi Cai)

An Augmented Reality-enabled Digital Twin System for Reconfigurable Soft Robots: Visualization, Simulation and Interaction

Zhongyuan Liao[a], Wanzhen Wei[b], Leihan Zhang[b], Yuer Gao[b], Yi Cai[a,b,c,*]

[a]*Division of Emerging Interdisciplinary Areas (EMIA), Academy of Interdisciplinary Studies, The Hong Kong University of Science and Technology, Hong Kong SAR, China*
[b]*Smart Manufacturing Thrust, Systems Hub, The Hong Kong University of Science and Technology (Guangzhou), Guangzhou, China*
[c]*Department of Mechanical and Aerospace Engineering, The Hong Kong University of Science and Technology, Hong Kong SAR, China*

Abstract

In the rapidly evolving field of soft robotics, the development of new materials, structural designs, and conceptual frameworks has led to the rise of soft robot technology, which is now moving towards a highly versatile modular architecture with potential uses across various industries. However, one of the main hurdles faced in this domain is the shape-morphing challenge, as existing visualization and simulation tools struggle to adequately represent the complex and continued deformation behaviors of soft robots. Furthermore, there is a distinct lack of intuitive, user-friendly platforms for visualizing and interactively controlling the shape-shifting capabilities of these robots. In response to these challenges, this paper introduces an innovative digital twin (DT) system for reconfigurable soft robots set within an augmented reality (AR) environment. This system facilitates a more natural and accurate depiction of 3D soft deformations and provides an intuitive interface for simulation. We utilize a parameterized curve-driven method to dynamically adapt the DT in the AR space, ensuring smooth transitions between various 3D shape-morphing states. We identify three fundamental shape-morphing patterns—stretching, bending, and twisting—and create advanced visualization tools to precisely demonstrate these morphological changes. To enhance the real-time representation of shape-morphing, we employ sensor fusion to detect and depict the soft robot's structural changes as parameterized curves. Our system is fully operational in an AR environment, empowering users to conduct immersive examinations and simulate reconfigurations of real-world soft robotic systems. The source code is released on https://github.com/yuanzero/DT-Reconfigurable-Soft-Robot.

Keywords:
Digital Twin, Augmented Reality, Human-Robot Interaction, Reconfigurable Soft Robot, Shape-morphing robots

*Corresponding author:
Email address: yicai@hkust-gz.edu.cn (Yi Cai)

1. Introduction

The burgeoning field of soft robotics, marked by the deployment of compliant materials, is characterized by robots that achieve locomotion primarily through the elastic deformation of their structural components. Owing to their inherent attributes such as significant flexibility, compliance, adaptability, and enhanced safety during human-robot interaction, soft robots have attracted increasing academic attention. With promising applications in sectors such as medical devices, wearable technology, and industrial automation, soft robotics stands at the forefront of interdisciplinary research [1].

In the contemporary landscape of industrial innovation, the principle of reconfigurability is gaining prominence, promoting the subdivision of large and complex systems into smaller, more manageable modular units [2]. Reconfigurable soft robots (RSRs) offer the unique ability to adapt to varying environmental and task-specific demands by reorganizing their modular constituents. This adaptability endows RSRs with advanced capabilities including self-assembly, self-repair, and autonomous actuation, while conferring advantages such as ease of maintenance, customizable configurations, scalability for mass production, and enhanced reusability [3]. Current research trajectories within the RSR domain are primarily dedicated to the exploration of modular design, simulation methodologies, fabrication techniques, interconnection dynamics, sensor integration, and control algorithms. A plethora of RSR prototypes have been developed, encompassing soft modular constructs akin to LEGO [4], chiral-lattice structures for locomotion [5], spherical RSRs [6], flexible robotic limbs [7], and origami-inspired RSR configurations [8]. Nonetheless, the establishment of comprehensive theoretical frameworks for the systematic design and operation of RSRs is still emerging, with existing designs predominantly oriented towards practical applications and lacking in sophisticated visualization and simulation techniques.

Digital twins (DT), conceived as digital analogues of tangible entities, emerge as a revolutionary technology within the industrial sphere, furnishing essential capabilities in the realms of visualization and simulation pertinent to practical deployments [9]. The concept of DTs was first introduced by Michael Grieves in 2002 as a model for product lifecycle management [10]. NASA and USAF first utilized DT as a multi-physics model-based and data-driven simulation, which was used for predictive aircraft maintenance [11]. As a cutting-edge technology in modern industry, DT is gaining widespread recognition from both academia and industry, as it facilitates effective monitoring, maintenance, and optimization of industrial systems, thereby enhancing their productivity and efficiency [12, 13]. Yet, the integration of such advanced technologies within the soft robotics discipline is challenged by the significant and intricate shape-morphing behaviors intrinsic to these entities.

To comprehensively document the intricate deformation behaviors characteristic of shape-morphing robots, two main approaches are employed including the utilization of physical model-based models and the integration of advanced sensing technologies, as shown in Table.1. Physical model-based methods exploit the intrinsic properties of materials and their foundational structural dynamics to accurately predict deformations. In this realm, Liu et al. [14] have demonstrated the use of a reduced-order model for the numerical simulation of shape-morphing surfaces, while Sun et al. [15] have introduced a physics-based model leveraging Cosserat rod theory, adept at handling the nonlinear

dynamics associated with substantial deformations.

Parallel to these developments, the domain of soft robotic sensing has been delineated into two primary categories: sensorization via devices and sensorization via soft materials [16]. Device-based sensorization encompasses both exogenous sensing methods, such as cameras and motion capture systems [17, 18], and endogenous approaches that incorporate off-the-shelf rigid sensors within soft robotic structures. These endogenous devices include a variety of sensors such as bendable flex sensors [19, 20], optical fibers [21], magnetic sensors [22], acoustic sensors [23] and distributed Inertial Measurement Units (IMUs) [24, 25], among others. Conversely, materials-based sensing strategies often employ sensors crafted from piezoresistive composites, including conductive nanoparticle-filled elastomers [26, 27], hydrogels [28], conductive liquids [29], and elastomeric waveguides [30]. Each sensing strategy presents distinct challenges. Exogenous sensing methods, while useful, are not seamlessly integrated into the robot's structure, thereby complicating proprioceptive and tactile sensing. Endogenous sensing with rigid devices, although innovative, faces mechanical interfacing challenges and limited design flexibility, often yielding non-intuitive feedback. On the other hand, sensors based on soft materials are susceptible to time-varying, hysteretic feedback, environmental sensitivities, and long-term reliability concerns. Moreover, the integration of sensing technologies into shape-morphing robots significantly enhances their DT representations, facilitating real-time deformation tracking.

Notwithstanding the advancements in sensing technologies, a significant impediment in DT systems is the accurate reconstruction of three-dimensional geometries. The prevalent methodologies for visual representation are fundamentally elementary, often depicted through rudimentary geometrical shapes such as curves [31, 32], planes [33], or simplified 3D surfaces [34, 35]. These methods inadequately represent the intricate 3D deformations inherent in robotic structures. Moreover, research focusing on the dynamic alterations in configuration, particularly in scenarios involving human interaction, remains notably limited.

Attribute	**Physical Model-based**	**Sensor Data-Driven**
Represented Method	Finite Element Analysis (FEA), Material Point Method (MPM)	Cameras, optical fibers, Soft sensors
Visualization	2D/3D geometry	curves [31, 32], planes [33], or simplified 3D surfaces [34, 35]
Response	Most offline, few real-time [36]	Real-time
Simulation	Enable	Most None
Interaction	Most None	Most None
Cost	High computational cost	Expensive device

Table 1: Comparison of two main DT methods.

Incorporating Augmented Reality (AR) within DT systems has the potential to enhance real-time informational displays, thereby providing a more intuitive interface for human-robot interactions and enriching the immersive experience within the realm of RSR. Through the integration of sensorized soft robots, Borges et al. [37] have delineated a conceptual framework aimed at shape reconstruction in the milieu of extended reality. Zhu et al. [38] have employed liquid crystal soft actuators and robots to facilitate a Mixed Reality (MR) environment enriched with visual, auditory, and haptic

interactions. Nonetheless, research endeavors leveraging AR to develop DTs capable of real-time visualization, simulation, and interaction with soft deformations remain scarce. The absence of a comprehensive, precise visualization, simulation, and interaction platform within the RSR domain significantly hampers the progression of the field.

Here, we introduce an innovative methodology for the synthesis of a DT tailored to a reconfigurable soft robot through the implementation of soft strain sensors and AR technology. Our proposed system facilitates the instantaneous and uninterrupted depiction of the robot's deformation within an AR milieu, empowering users to adjust the configuration of the soft modular components. Additionally, it provides the capability to simulate these alterations in AR to accommodate a diverse array of functional task demands.

There are three key benefits of human interaction with soft robots: 1) Enhanced Reception of Feedback: Human interaction with soft robots allows for a more intuitive and effective reception of feedback in DT system. Users can better perceive and understand the robot's responses, leading to improved collaboration and communication between humans and robots. 2) Reconfiguration through AR interaction: The integration of AR technology enables users to modify the robot's configuration interactively. This adaptability allows for a more tailored experience, where users can visualize and implement changes in the configuration of the soft robot. 3) Realistic simulation in context: By simulating configurations within real-world environments, users can better understand how reconfigurable soft robots will perform in their actual working contexts. This capability fosters a deeper connection between the virtual and physical worlds, allowing more effective planning, training, and operational efficiency.

2. Frameworks

The framework of the DT system for RSR is designed to offer a user-friendly platform that facilitates seamless visualization, simulation, and interaction. This allows users to accurately perceive the deformation of RSR, as well as simulate its configuration with intuitive interaction. The framework consists of some primary components: parametric curve-based visualization, sensor-fusion method, simulation and control strategy, and human interaction as depicted in Fig.1, and the details are shown in Section.3.

In the modular design and fabrication phase, reconfigurable robots are engineered to exhibit three primary deformation modalities: stretching, bending, and twisting. This modular methodology facilitates easy reconfiguration for diverse tasks and environments through the use of interchangeable modules that can be connected or disconnected to achieve specific deformation patterns. This approach minimizes the necessity for extensive customization and accelerates prototyping.

Parametric curve-based visualization employs parametric curves to depict the physical postures of soft robots, enabling continuous deformation within the AR environment. The integration of AR technology provides an intuitive and immersive interface for visualizing robot configurations, allowing for virtual simulations before physical implementation.

Sensor fusion is integral to the DT System, combining sensor data to depict real-time, continuous deformation in an AR setting. The DT system utilizes a cost-effective and straightforward strain gauge sensor to detect and convey the robots' deformation

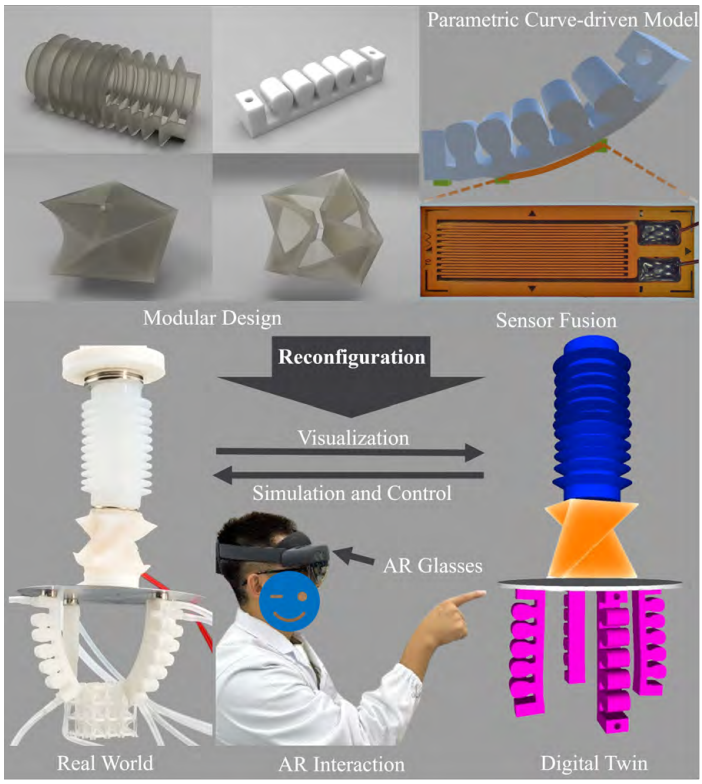

Figure 1: The framework of the AR-enhanced DT system for reconfigurable soft robots.

patterns. This data is processed and mapped onto a parametric curve, representing the soft robots' postures. This mapping facilitates real-time deformation control of the DT robot, mirroring movements in the real world and ensuring accurate, responsive control within the AR environment.

In the process of reconfiguration, users can engage with the AR-based DT system, facilitating simulate to RSR's configuration and deformation. Upon completing the simulation, they can implement the validated configuration in the real physical environment.

3. Methodology

3.1. In-situ Visualization Theory

The concept of parametric curve-based visualization and control has been utilized in this approach, with a specific emphasis on the Bezier curve model. This model consists of n control points and plays a crucial role in determining the deformation patterns of the robot. The curve is comprised of several bones that are distributed along its points, which define the location and orientation of the robot's modules.

The bone functionality in Blender serves as a crucial component in the rigging and animation process. It represents a joint or segment within a skeletal structure and allows for the manipulation and control of 3D models. By adding, editing, and positioning bones, complex armatures can be created to accurately deform and animate characters or objects. This capability is particularly useful when working with soft robotic modules, where the bone framework can be utilized to simulate the flexible and dynamic behavior of these modules.

Fig.2a illustrates the weight painting process applied to a bone, revealing its impact on the deformation of the soft robot module. This weight painting technique involves assigning distinct weights to each vertex of the module, taking into consideration the distance. The closer the vertex is to the bone, the higher the assigned weight, which determines the extent to which the movement of the associated bone affects that particular vertex.

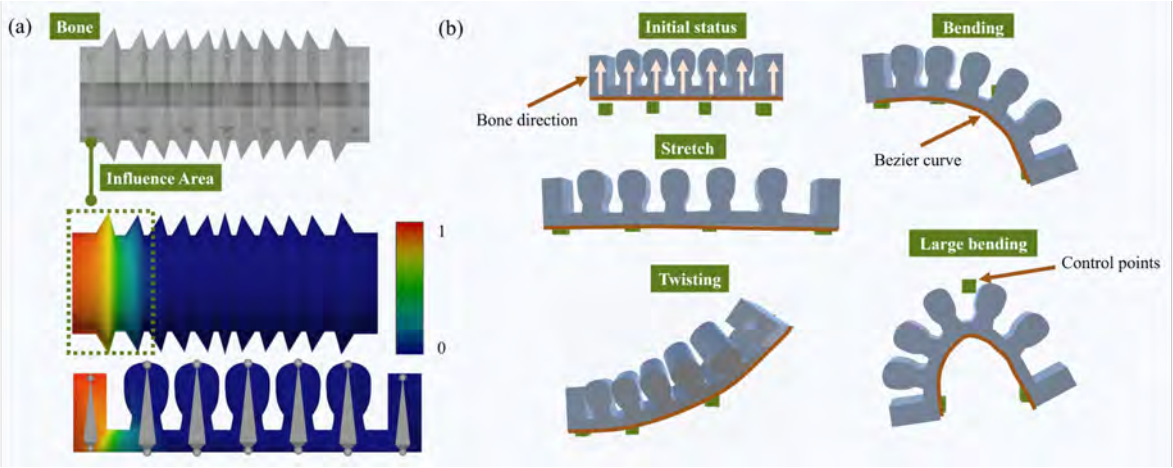

Figure 2: (a) Weight paint of a bone on a soft robot module. The color-coded weight distribution determines the influence of the bone on the deformation of the module. (b) The continuous deformation with different positions of control points (the green cubes).

The bone-based model can be subsequently exported to Unity for further development. By using Blender's bone system, intricate skeletal structures can be constructed to facilitate continuous deformations of soft robots. This enables the user to establish precise control over the model's movements and expressions. Once exported to Unity, the bone structure is attached to the control point of the parametric Bezier curve. By manipulating the control points, the parameterized curve is altered, and the corresponding bones on the curve are also modified, ultimately resulting in continuous deformation of the modules. The seamless integration of bone functionality between Blender and Unity enhances the overall workflow and facilitates the creation of visually compelling and interactive 3D experiences.

The equation for the Bezier curve $B(t)$ is:

$$B(t) = \sum_{i=0}^{n} P_i B_i^n(t) \tag{1}$$

where P_i are the position of control points, n is the degree of the curve, and $B_i^n(t)$ are the Bernstein basis polynomials defined as:

$$B_i^n(t) = \binom{n}{i}(1-t)^{n-i}t^i \tag{2}$$

where the parameter t is in the range [0,1].

The tangent vector at any given point on the curve is given by its first derivative $B'(t)$.

$$B'(t) = n \sum_{i=0}^{n-1} (P_{i+1} - P_i) B_i^{n-1}(t) \tag{3}$$

where P_i are the control points, n is the degree of the curve, and $B_i^{n-1}(t)$ are the Bernstein basis polynomials defined as:

$$B_i^{n-1}(t) = \binom{n-1}{i} (1-t)^{n-1-i} t^i \tag{4}$$

Here, a variable $PB = [PB_0, PB_1, ..., PB_i, ..., PB_m]$ is utilized to represent the location of the chamber's bone, where m is the number of the bones, each PB_i denotes the position of a bone on the Bezier curve, represented as:

$$PB_i = B(t), t = i/m \tag{5}$$

For simplicity, the bones are arranged in equal distance. By adjusting this variable PB, it is possible to drive the corresponding part of the robot to deform as required, thereby enabling a high degree of control over the robot's configuration and movement patterns.

Each bone on the curve is set to be vertical to the curve. The normal vector is the vector perpendicular to this tangent vector. In the 2D case, the normal vector $N(t)$ can be easily calculated by rotating the tangent vector by 90 degrees. Specifically, if $B'(t) = (x, y)$, then $N(t) = (-y, x)$ or $N(t) = (y, -x)$, depending on the orientation. In the 3D case, there is no unique normal vector. For 3D curves, normal vectors are infinite in the normal plane. Thus, a unique normal direction is defined by the tangent direction, which is a 90° rotation around the x-axis. It is represented as:

$$N = R \cdot B'(t) \tag{6}$$

where R is the rotation matrix. In the case of 3D curves, the determined tangent line possesses two distinct directions. In order to maintain a continuous deformation, it is necessary to impose constraints on tangent directions, ensuring that the crossing angle between adjacent tangent directions remains below 90°.

Fig.2b illustrates the deformation that arises when altering the positions of control points. This representation showcases the Bezier curve, a space curve determined by the control points, visually represented as the red line. Moreover, the control points are visually denoted by green cubes. Additionally, the blue arrows serve to indicate the orientation of the bone, which is positioned orthogonally to the Bezier curve. The user has the capability to manipulate the cube, which represents the positions of the control points, thereby modifying the deformation of the soft robot module. By displacing the cube in a specific direction, the module can be stretched. Similarly, bending can be achieved by moving the cube within the plane, while twisting can be accomplished by displacing the cube in three-dimensional space.

The process of twisting deformation is a unique transformation that differs markedly from standard stretching and bending visualization modeling. We present an innovative two-phase algorithm that orchestrates the self-twisting of a geometric entity through precise adjustments to its mesh vertices while maintaining the object's original geometric integrity. The algorithm comprises an initial phase of vertex rotation to set the stage

for the deformation, followed by a subsequent phase that involves the computation of scaling factors to actualize the desired transformation. The intuitive illustration of the twisting mechanism is shown in Fig. 3.

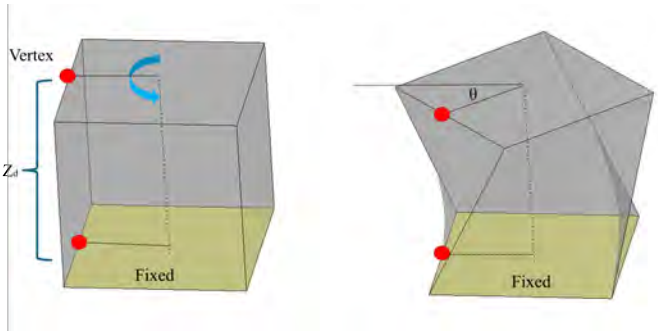

Figure 3: Illustration of twisting mechanism. For a twisting module, one bottom face is fixed, and the vertex beside the fixed surface rotates an angle θ, related to the distance to the fixed surface z_d.

In the first phase, each mesh vertex is rotated around a predefined axis by a calculated angle. This angle is proportional to the vertex's z-axis distance from a reference point, designated as z_o. The rotation serves as the preliminary step for the deformation process. The mathematical relationship governing the twist angle for each vertex, θ_z, based on its normalized z-axis distance, z_d, is given by:

$$z_d = \frac{z_{vertex} - z_o}{z_{max} - z_o} \tag{7}$$

$$\theta_z = z_d \cdot \theta \tag{8}$$

where θ represents the maximum twist angle. The second phase involves determining a scaling factor for each vertex by comparing its original position to its post-rotation position. This scaling is critical to ensure that the deformation conforms to the geometric proportions of the original object. The vertices are then scaled accordingly to achieve the final self-twisting effect.

Through this algorithmic approach, the manipulation of the object's mesh is systematically controlled, enabling the realization of a complex twisting deformation. The method delineated here affords precise control over the deformation, allowing for the creation of intricate twisted geometries that are consistent with the desired transformational objectives.

3.2. Sensor Fusion Method

A succinct sensor fusion approach is introduced in order to accurately measure the actual deformation of various types of modules in their natural environment. This method relies solely on the utilization of a strain gauge (SG), a simple yet effective sensor, see Fig.4a. The operational principle of the resistance strain gauge is predicated on the strain phenomenon, wherein the resistance value of a conductor or semiconductor material alters proportionally with its mechanical deformation under external forces, commonly referred to as the "strain effect". By affixing the strain gauge to the material to be measured, it flexes in accordance with the strain experienced by the material, causing the internal metal foil to also bend correspondingly. A key advantage of the

proposed soft module is its straightforward deformation patterns, each characterized by a unique and distinct form. Consequently, the localized deformation measured by the strain gauge effectively represents the overall deformation of the entire module.

3.2.1. Bending Measurement

In the theory of strain gauge (SG) measurement, the relationship between strain and the corresponding change in resistance can be expressed using the equation:

$$\epsilon = \frac{\Delta R}{R} \cdot \frac{1}{S} \tag{9}$$

Here, ϵ represents the strain, ΔR represents the change in resistance, R represents the initial resistance, and S represents the gauge factor. The gauge factor, denoted as S, is a characteristic parameter of the strain gauge that indicates the ratio of the relative change in resistance to the applied strain.

To incorporate bending measurement using a strain gauge, the equation can be modified to account for the bending strain. Bending strain is a result of the curvature or deflection of the material under external forces. The modified equation for bending strain can be expressed as:

$$\epsilon_b = \frac{\Delta R_b}{R} \cdot \frac{1}{S_b} \tag{10}$$

where ϵ_b represents the bending strain, ΔR_b denotes the change in resistance due to bending, R signifies the initial resistance, and S_b represents the gauge factor for bending strain.

When both bending and axial strains are present, the total strain can be calculated as the sum of the bending strain (ϵ_b) and the axial strain (ϵ_a):

$$\epsilon_{\text{total}} = \epsilon_b + \epsilon_a \tag{11}$$

Similarly, the total change in resistance (ΔR_{total}) can be obtained by adding the change in resistance due to bending (ΔR_b) and the change in resistance due to axial strain (ΔR_a):

$$\Delta R_{\text{total}} = \Delta R_b + \Delta R_a \tag{12}$$

When the axial strain is imperceptible, it becomes possible to ascertain the change in resistance, thereby enabling the assessment of the effect of bending when the object is connected to the flexible module. With the sensor bending, the corresponding resistance value changed in Fig.4d.

The strain gauge measurement theory provides a robust framework for accurately assessing deformation and strain experienced by various modules in real-world scenarios. In practical applications, the change in measured resistance is converted into a voltage signal V using a Wheatstone bridge circuit, as depicted in Fig.4b. This voltage signal can then be amplified and processed for further analysis and interpretation. Different deployment layouts are utilized for the various modules. In the bending module, the sensor is positioned flatly on the bottom face, allowing it to directly reflect the bending angle when the module deforms. In the stretch module, the strain gauge is placed on the gap between folds, enabling it to register changes in length. In the twisting module,

the strain gauge is positioned on the side face to correspondingly register twists. By analyzing the output voltage of the strain gauge, the true deformation of the different modules can be easily determined.

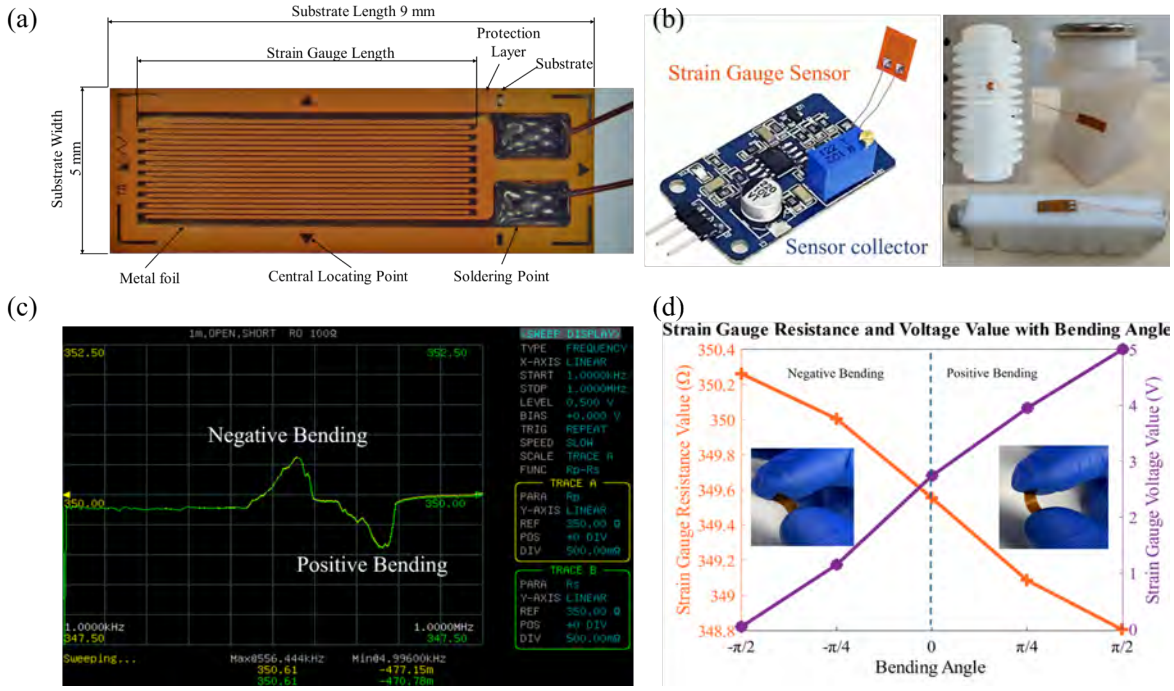

Figure 4: (a) The structure design of the strain gauge sensor. (b) The sensor deployment of three modules with the data collection module. (c) The measurement curve using the LCR meter. (d) The illustration of the fluctuation of the strain gauge resistance value and the voltage output value in correlation with varying bending angles.

3.2.2. Calibration

The data collected from sensors requires processing and analysis. The first step involves calibration to establish a correlation between the sensed values and the position of the control point. Within each module, specific deformation statuses are selected as points along the known trajectory. These points are used to construct a continuous trajectory for each control point using a Bezier curve. This is achieved through reverse calculation. Let $PT = [PT_0, PT_1, PT_2, ..., PT_n]$ represent the set of known trajectory points, where n is the total number of known trajectory points.

The goal is to determine the control points $C = [C_0, C_1, C_2, ..., C_n]$ that enable the generation of a Bezier curve passing through the given trajectory points, with $PT_0 = C_0$ and $PT_n = C_n$.

The control points C are calculated using the equation:

$$C_i = \binom{n}{i} \cdot PT_i \tag{13}$$

where C_i represents the i-th control point, PT_i denotes the i-th known trajectory point, and $\binom{n}{i}$ represents the binomial coefficient.

Once the control points C are determined, the original Bezier curve formula PT is used to compute the fitted trajectory points within the given parameter T. The formula is as follows:

$$PT(T) = \sum_{i=0}^{n} \binom{n}{i} \cdot (1-T)^{n-i} \cdot T^i \cdot C_i \tag{14}$$

The sensor fusion method incorporates a fitting function to establish the relationship between the position of the control points (TC) and a voltage signal (V), which can be expressed by the equation:

$$T = f(V) = mV + c, T \in [0, 1] \tag{15}$$

In this work, a linear mapping is utilized, where m represents the slope and c represents the y-intercept of the line. By mapping the parameter V to parameter T, a smooth trajectory can be generated, with each input V corresponding to a specific deformation. The fitted trajectory points obtained through this process serve as a representation of a smooth trajectory passing through the given set of trajectory points. This fitting function enables the integration of sensors with the DT system, allowing for accurate visualization of the same deformation observed in the real world. Fig.5 illustrates a comparison between the observed physical deformations in the soft modules and the analogous deformations within their virtual equivalents as part of a DT framework. This system enables users to engage in an interactive manipulation of the soft module through AR interfaces, thereby allowing for the pre-emptive simulation of functional behaviors prior to actual operation. Such a feature facilitates the exploration and assessment of diverse configurations across a spectrum of potential applications.

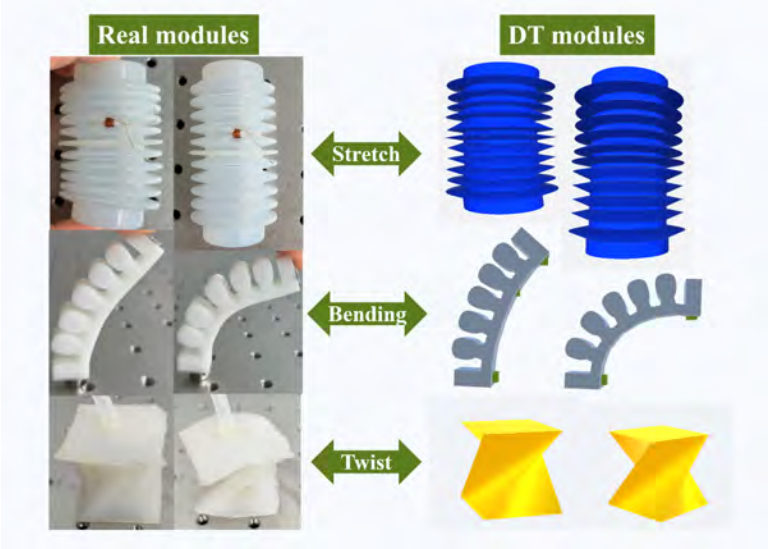

Figure 5: The real deformation of the soft modules along with their DT.

3.3. Simulation and Control

In addition to the visual representation and manipulation of the Bezier curve and control points, the simulation and control aspect of this integration offers advanced

features for testing and refining the behavior of the soft robot module. The simulation module incorporates principles from control theory, enabling the implementation of control algorithms to govern the movement and deformation of the soft robot.

Control theory plays a crucial role in the simulation of the soft robot module, providing a framework for designing feedback control systems that regulate the module's behavior in response to various inputs and disturbances. One of the fundamental concepts in control theory, the PID (Proportional-Integral-Derivative) controller, can be employed to stabilize the deformation and movement of the soft robot module by adjusting the positions of the control points in real time.

The PID controller utilizes the error signal, which represents the difference between the desired deformation or movement trajectory and the actual state of the soft robot module, to compute control signals that drive the system towards the desired behavior. The control signals are determined based on the proportional, integral, and derivative terms, each of which contributes to the overall control action in a specific manner. The control signals generated by the PID controller can be directly mapped to the adjustment of control points along the Bezier curve, enabling precise and dynamic control over the deformation and movement of the soft robot module. The integration with connection technology (detail in Section.4.2) allows for the real-time execution of these control signals, resulting in immediate feedback on the module's behavior and performance.

The error signal, denoted as $e(s)$, represents the difference between the desired shape or deformation of the soft module and its actual state at time s. The control signals generated by the PID controller can be applied to the positions of the control points to drive the soft module toward the desired deformation.

The PID control output $u(s)$ at time s is computed as the sum of proportional, integral, and derivative terms:

$$u(s) = K_p e(s) + K_i \int_0^s e(\tau) d\tau + K_d \frac{de(s)}{dt} \tag{16}$$

where K_p, K_i, and K_d are the proportional, integral, and derivative gains, respectively.

The control output $u(s)$ can be interpreted as the adjustment to the positions of the control points of the Bezier curve. For example, the control output can be used to modify the x and y coordinates of the control points, thereby deforming the soft module.

The new position of a control point at time $s+1$ can be computed based on the control output $u(s)$ and the previous position of the control point:

$$x_i(s+1) = x_i(s) + u_x(s), y_i(s+1) = y_i(s) + u_y(s), z_i(s+1) = z_i(s) + u_z(s) \tag{17}$$

In these equations, $x_i(s)$, $y_i(s)$, and $z_i(s)$ represent the current x, y, and z coordinates of the control point P_i, while $u_x(s)$, $u_y(s)$, and $u_z(s)$ are the components of the control output $u(s)$ that affect the position of the control point. By manipulating the positions of the control points in this way, the soft module can dynamically deform in response to the output of the PID controller, allowing for real-time adjustment of its shape and trajectory in 3D space.

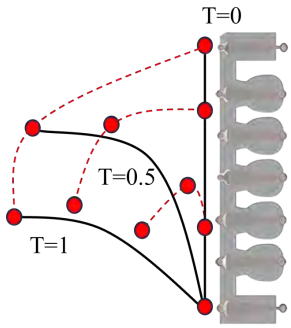

Figure 6: The illustration of the trajectory $PT(T)$ of the control points.

To simplify the control strategy, the trajectory of each control point actuated by pressure can be represented as a parameterized curve, $PT(T)$, where T is the parameter defining the position of the control point, shown in Fig.6. By integrating with PID control, the parameter T can be computed as:

$$T_i(s+1) = T_i(s) + u_T(s) \tag{18}$$

Here, $T_i(s)$ represents the current value of T defining the coordinates of the control point P_i, and $u_T(s)$ is the component of the control output $u(s)$ influencing the trajectory of the control point. By establishing a relationship between the components of the control output $u_T(s)$ and the operation of the valve, the soft module can be manipulated to achieve the desired position. This relationship is defined by the equation:

$$P_{in} = K \cdot u_T(s) \tag{19}$$

In this equation, P_{in} represents the pressure input exerted on the soft module, which can be a positive or negative pressure source, and K denotes the proportional gain that correlates $u_T(s)$ to the pressure input. The proportional valve is responsible for regulating the pressure based on the error signal generated by the PID controller, thereby adjusting the pressure applied to the soft module in response to variations in the error signal. Through the integration of these mechanisms, the soft module is effectively driven towards the desired position.

For the soft robot gripper, controlling input pressure smoothly is essential to prevent damage to the soft module. Thus, the criteria for selecting the proportional, integral, and derivative gains were established to ensure that when the sensor detects an overshoot, the pressure is reduced and then gradually adjusted toward the target status. Currently, the PID parameters we employed are designed to ensure safe interaction with the soft module, resulting in a smooth deformation response.

The adjustment strategies for PID control parameters are significantly influenced by the specific operational contexts. For tasks requiring precision, such as the grasping of small objects, it is essential to set a low proportional gain K_p to minimize overshoot while moderately adjusting the integral gain K_i to eliminate steady-state errors. Additionally, increasing the derivative gain K_d can enhance the system's sensitivity to rapid changes. Conversely, in scenarios necessitating swift grasping, a judicious increase in proportional gain K_p can improve the system's response speed, while maintaining the

integral gain K_i at a moderate level helps avoid excessive steady-state errors. The derivative gain K_d should also be increased to mitigate oscillations induced by rapid changes. When handling heavy objects, the proportional gain K_p should be set at a moderate or slightly higher value to ensure sufficient grasping force, while the integral gain K_i may be slightly elevated to maintain stability; the derivative gain K_d should be set at a moderate level to prevent significant reactions to load variations. In the context of grasping flexible materials, a lower proportional gain K_p facilitates a gentle grasping process, while a moderate derivative gain K_d aids in controlling dynamic changes. For dynamic environments, proportional gain K_p should be adjusted to a moderate or slightly higher level to enable rapid adaptation to environmental changes, while keeping the integral gain K_i low helps avoid the introduction of unnecessary steady-state errors; increasing the derivative gain K_d can enhance the system's responsiveness to dynamic variations. Finally, in multi-tasking operations, PID parameters should be flexibly adjusted according to the requirements of the current task to achieve precise control and optimize the performance of the soft robotic gripper.

3.4. AR-enhanced Intuitive Interaction Design

The intuitive interface is a vital component of human-robot interaction (HRI), significantly influencing the efficiency and ease of use of the DT system. An ideal interface for HRI should have three essential functions: visualization, simulation, and control. Visualization provides real-time feedback on the robot's position, orientation, and deformation. The simulation module is described as crucial for accurately representing the robot and its environment, enabling users to visualize and interact with the robot in a virtual setting, and facilitating experimentation and optimization of the robot's configuration before real-world implementation. Control is also emphasized, allowing users to efficiently manipulate the RSR's configuration and deformation for various tasks and operations. Hololens 2, a mixed-reality headset developed by Microsoft, equipped with advanced sensors and cameras to track the user's gestures, is utilized in this work, offering an immersive experience by blending the virtual and real world. This technology is lauded for enabling natural and intuitive interactions with virtual objects and environments, making it an ideal platform for HRI. Unity, a popular game development engine, is utilized to create the AR environment and user interface for controlling the robot arm, and the Mixed Reality Toolkit (MRTK) for Unity is employed to simplify the development of mixed-reality applications using the Hololens 2 headset. The new interaction method allows users to directly manipulate the RSR with intuitive gestures.

The reconfigurable soft robot (RSR) interface is depicted in Figure 7. It consists of two main modules, namely the visualization module and the control penal. The control panel offers several switches that allow users to select the specific module they wish to control. The control hardware can be found in Fig.9. Within each soft module, the status can be chosen from three options: open, hold, and release. The open status corresponds to opening the valves that connect to the high-pressure or vacuum source. On the other hand, the hold status involves closing all valves and maintaining the previous state. Lastly, the release status signifies closing the valves connected to the high-pressure or vacuum source and opening the valves to the atmosphere. Additionally, the control panel includes two toggles. The first toggle activates the PID control, which can be used to regulate the modules' shape-morphing. The second toggle determines whether the DT system should continue reading information from the

deformation sensors. This feature enables real-time monitoring and adjustment of the RSR's performance during operation. Overall, the RSR interface provides a comprehensive control mechanism, allowing users to manipulate and customize the soft robot's behavior according to their specific requirements. Users have provided feedback indicating that the interface is user-friendly, allowing for easy manipulation of the virtual soft modules within the DT system.

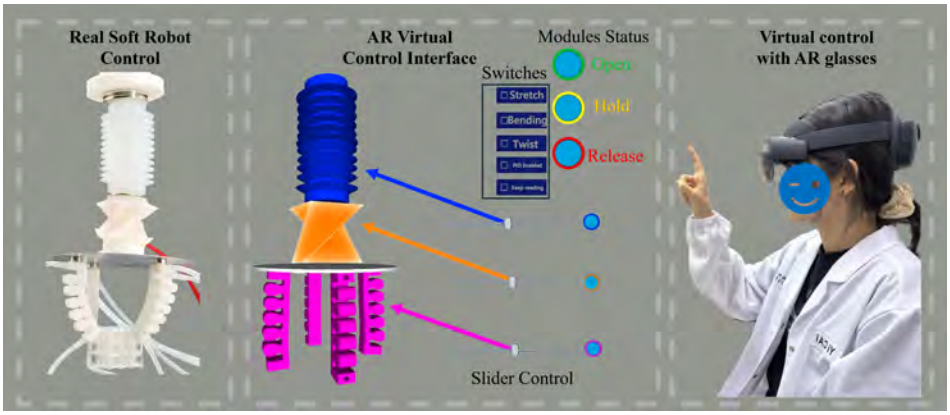

Figure 7: The AR-based interface for RSR.

4. Platform Implementation

4.1. Module design and fabrication

The tripartite modular design is derived from the fundamental motion patterns observed in conventional soft robot designs. This design approach employs additive manufacturing and molding techniques to effectively fabricate the final product. The stretch module is inspired by the folding zones of Chinese lanterns, allowing for longitudinal stretching. The twisting module incorporates a propeller-like structure consisting of two parallel square plates connected by four twisted blades. By directing airflow through the chamber, an unbalanced force distribution is created, resulting in twisting deformation. Conversely, the bending module utilizes a chamber with a wider upper section and a narrower lower section to induce bending deformation. These three modules, as illustrated in Fig. 8, collectively contribute to the overall functionality of the tripartite modular design. More design and fabrication details can be referred to the previous works [3, 39]. For convenience assembly and disassembly, the magnet connection is utilized.

4.2. Control Platform

The control module, as depicted in Fig.9, comprises various components for regulating the system. The air valve is utilized to manage the flow of high-pressure, vacuum, and atmospheric connections. Relay switches are employed to govern the valves, with the Arduino MEGA serving as the controller for these switches. The proportional valve is utilized to control the input pressure. The sensor collector is responsible for gathering deformation data from the bending sensor, converting it into voltage, and transmitting it to the Arduino. Additionally, the ESP32 acts as an intermediary for receiving user

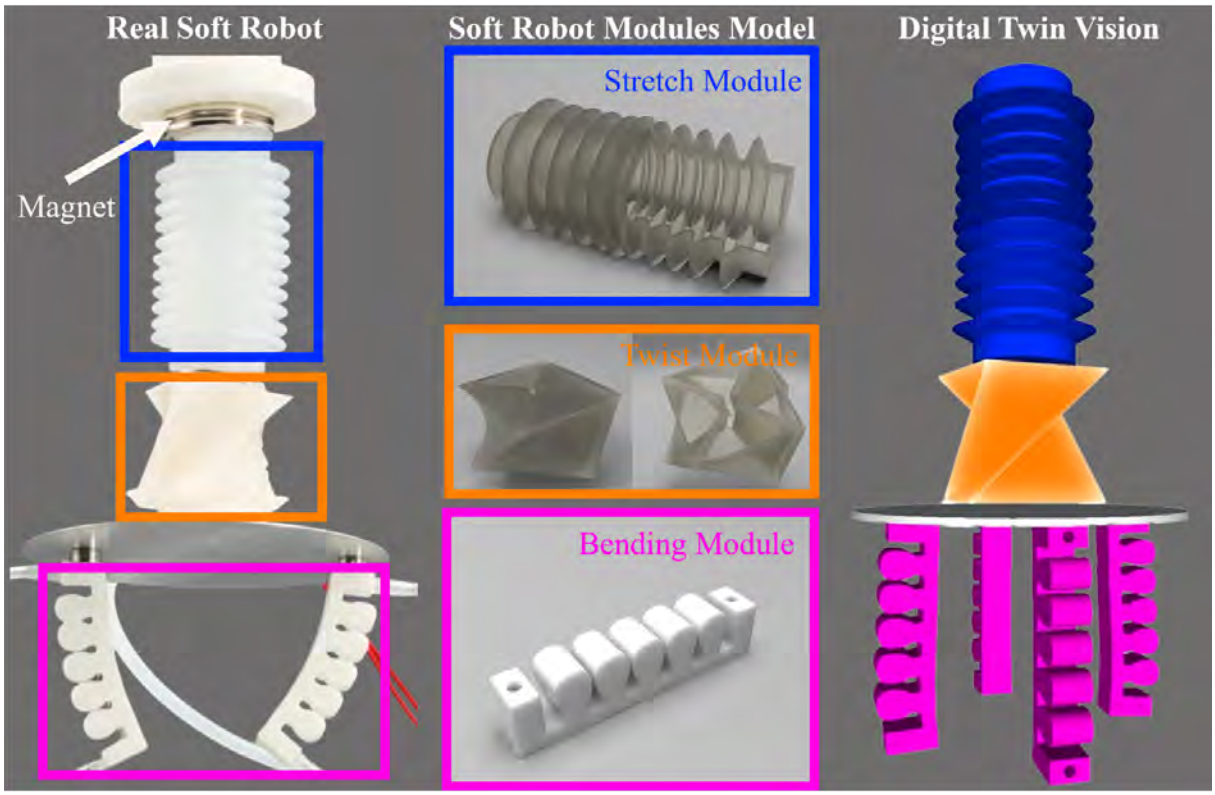

Figure 8: The structure design of three basic soft modules.

input and transmitting sensor data to the DT system. Communication between the HoloLens and ESP32 occurs via WiFi.

The practical control performance is tested on a real control platform with a proportional valve. The results are depicted in Fig.10, demonstrating the feasibility of the proposed PID controller in achieving the desired shape and deformation of the soft module. The precise control component has been integrated with the geometry module into a single class within the code implementation. Consequently, upon the reconstruction of the modules, regardless of whether the number of modules is increased or decreased, the control module remains associated with the geometry module.

4.3. Spatial Anchor for AR

The integration of AR with a physical soft robot poses a challenge in aligning virtual objects with the tangible environment. To address this, a spatial anchor is utilized to establish a virtual point in a three-dimensional space that is affixed to a tangible object or location. This anchor preserves the orientation and location of AR content in the tangible world, even when the camera is in motion. Unlike visual markers that trigger AR experiences, spatial anchors serve as a reference point for all other objects in the AR environment. The illustration of the spatial anchor is shown in Fig.11.

In order to determine the position of a virtual object in the global coordinate system, it is necessary to know its position and orientation relative to the spatial anchor in the local coordinate system. In this study, the position (P_l) and orientation (R_l) of the virtual object with respect to the spatial anchor are predetermined in Unity scenes and can be adjusted through human interaction. The 3×3 rotation matrix R_l represents

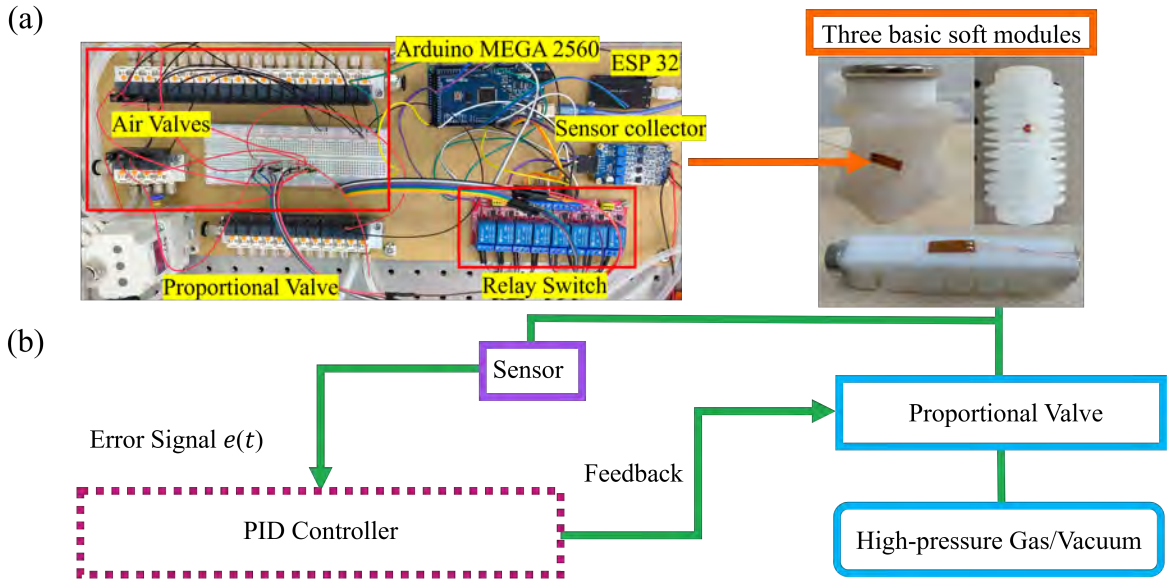

Figure 9: (a)The control hardware.(b) The control logic.

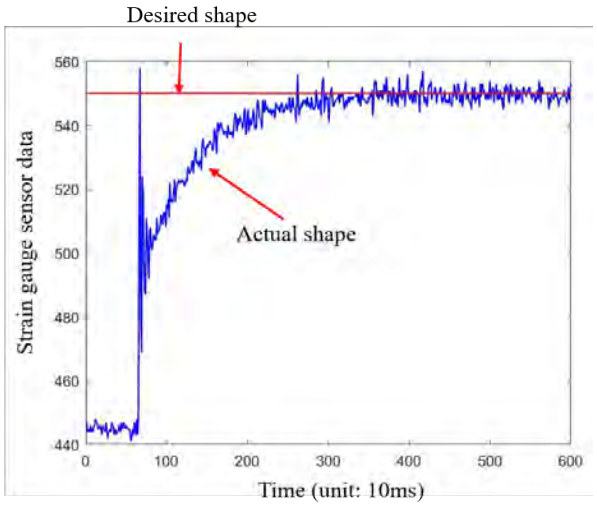

Figure 10: The control result based on the PID controller, with the y-axis representing strain gauge sensor data collected by an Arduino device. The sensor values, within the range of 0 to 1023, were subsequently mapped to a 0 to 5V range. The x-axis denoted the temporal progression of the experiment, with a sampling frequency of 100 Hz. The desired target deformation was depicted by a red line, contrasting with the actual sensor data illustrated by a blue line. Upon the occurrence of external stimuli, there was a rapid increase in module deformation surpassing the target shape, followed by a subsequent decrease and eventual convergence towards the desired deformation.

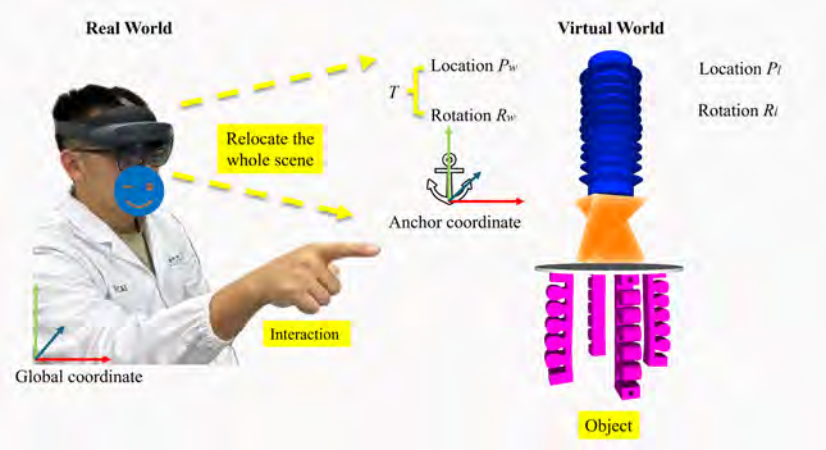

Figure 11: Illustration of the transformation between the virtual world and the real world using spatial anchor.

the orientation of the virtual object relative to the spatial anchor and can be computed using Euler angles or quaternions. Euler angles define the virtual object's orientation through three angles of rotation around the x, y, and z axes, while quaternions provide a more concise representation of orientation using a four-dimensional vector.

A homogeneous coordinate in a 4x4 metric (G_l) can be utilized to represent the local gesture, including the position and orientation with respect to the spatial anchor:

$$G_l = \begin{bmatrix} R_l & P_l \\ O(1 \times 3) & 1 \end{bmatrix} \tag{20}$$

The transformation process that maps the local G_l to the global G_w can be expressed as:

$$G_w = T \cdot G_l \tag{21}$$

where T is a 4x4 homogeneous transformation matrix:

$$T = \begin{bmatrix} R_w & P_w \\ O(1 \times 3) & 1 \end{bmatrix} \tag{22}$$

Here, R_w is a 3x3 matrix that characterizes the orientation, and P_w is a 3x1 vector that denotes the position of the spatial anchor with respect to the global coordinate system. It should be noted that the global coordinate system is located in the real world, while the local coordinate system is in the virtual scene. Through Eq. 21, the virtual world is aligned with the real world, allowing users to modify the location of the entire virtual scene by adjusting the anchor's position through AR interactions.

5. Demonstration

To demonstrate the superiority of the proposed DT (DT) system, an accuracy experiment was first conducted, as illustrated in Fig. 12, with the corresponding data presented in Table 2. This evaluation focused on the deformation of soft modules, where the deformation of the physical entity was directly mirrored by its virtual counterpart,

maintaining an identical scale. To quantify the deformation, distinct measurement methods were designed for each of the three soft modules. For the stretch module, the deformation was quantified by recording the change in the module's length L. We set the length of the initial stretch module as 1. For the bending module, the deformation was represented by the cross angle, denoted as β, between the endpoint and the perpendicular line. In the case of the twisting module, the cross angle θ between the line of intersection on the bottom face and the horizontal line was employed as the deformation measure. Simultaneous capture of the figures was ensured for each pairing of virtual and real entities. It is important to note that the captured figures may exhibit some distortion, as the HoloLens 2 is not specifically designed for high-fidelity camera capture.

Table 2 presents a comparison of the deformation degree of stretch, bending, and twisting modules, between the physical entity (PE) and the virtual entity (VE), emphasizing the high accuracy of the proposed DT system. The data in the table are listed from small to large deformation as same as the Fig.12 in each item. The high accuracy is demonstrated by the low error percentages, even approaching 0%. A slightly higher error is observed in bending and twisting modules, due to the more complex nature of these deformation patterns, which exhibit greater nonlinearity. Additionally, the measurement of angles, being more sensitive than length measurements, contributes to the observed discrepancies. The size accuracy of the virtual entities is maintained due to the use of the same geometric model as the real soft module, allowing users to perceive both as having equivalent dimensions. Regarding spatial precision, the spatial anchor described in Section.4.3 ensures that the virtual model is accurately embedded within the real world.

	Stretch Length L			Bending Angle $\beta(^\circ)$			Twisting Angle $\theta(^\circ)$		
PE	0.72	1.00	1.43	8	14	31	40	53	64
VE	0.71	1.00	1.41	8	13	29	42	53	66
Error (%)	1.39	0.00	1.40	0.00	7.14	6.45	5.00	0.00	3.13

Table 2: Deformation degree comparison between the physical entity (PE) and virtual entity (VE), and the corresponding accuracy error (%).

The DT framework is an intricate construct, meticulously devised to incorporate a trio of essential capabilities: advanced visualization, comprehensive simulation, and dynamic interaction. The forthcoming case study is designed to provide a thorough examination of the interoperability and practical effectiveness of these integrated features.

Initially, the invocation of the DT's foundational elements initiates a complex visualization framework, which is instrumental in providing a real-time, perspicuous visual account of the system's operational condition, as depicted in Figure 13a. This is succeeded by the simulation aspect of the DT, meticulously delineated in Figure 13b, which progresses through a deliberate sequence of stages. These include Configuration Selection, Deformation Simulation, Reconfiguration Execution, and Module Actuation. The simulation function plays a critical role in augmenting operational performance by preemptively validating system feasibility, thereby mitigating potential issues such as mechanical collisions or ineffective configurations that could impede the system's ability to interact with objects. This proactive approach ensures a streamlined and error-free

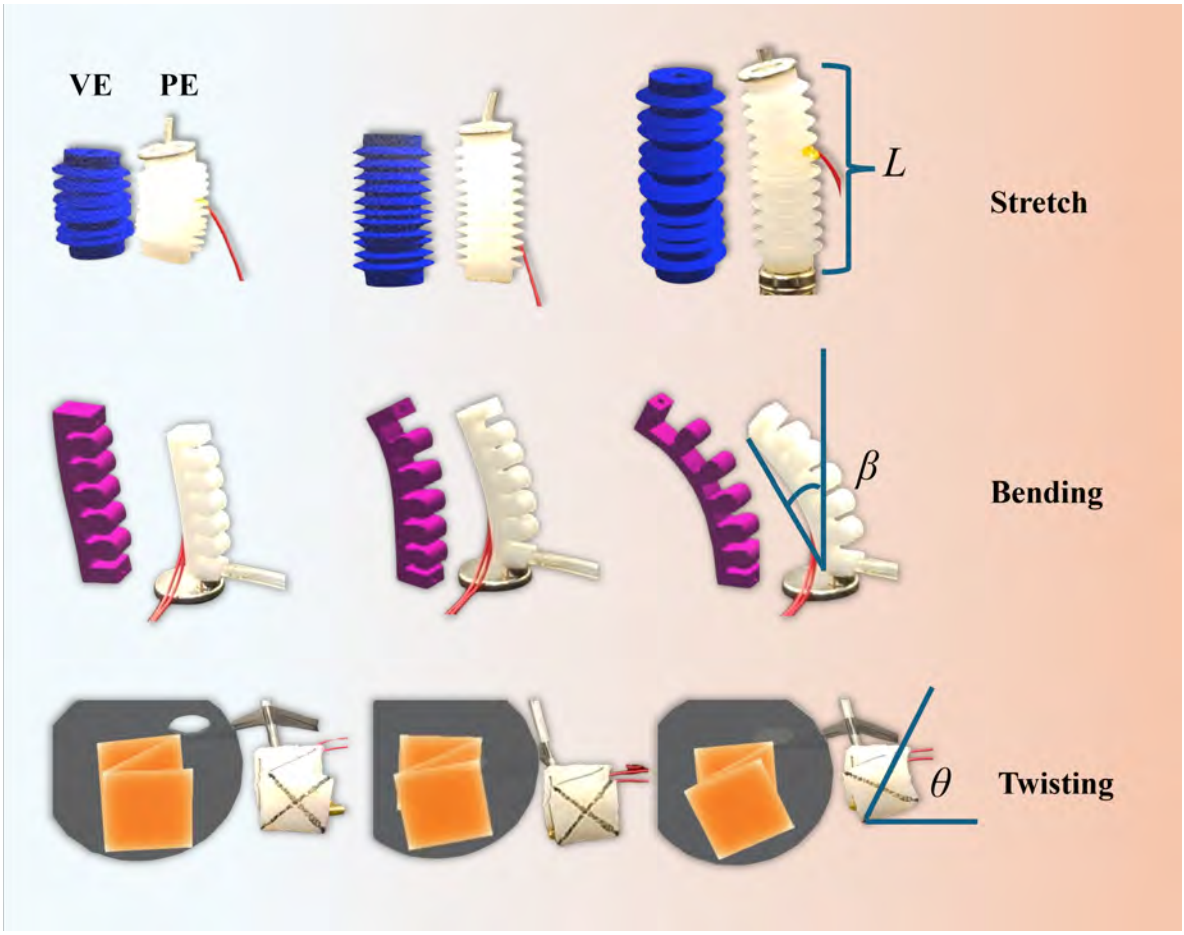

Figure 12: The accuracy experiment for soft modules involved simultaneous deformation of both the physical entity (PE) and virtual entity (VE) at the same scale. The deformation degree increases from the left to right. All the figures were caught by Hololens 2, where human can see the virtual and real entity in the AR vision. The deformation degree for the three basic soft modules was represented by the module length L, bending angle β, and twisting angle θ. All data were collected concurrently for each PE-VE pair.

operation before actual deployment, enhancing efficiency and safety within the system's real-world application.

Furthermore, the DT framework facilitates a user-friendly interaction layer, depicted in Figure 13c, allowing for gestural inputs that enable users to effortlessly modify and simulate structural changes within the digital environment. This integration of visualization, simulation, and interaction is pivotal, forming the DT system's foundation, and the case study's objective is to rigorously scrutinize these components to validate their synergy and effectiveness in a real-world application scenario.

To further elucidate the advantages of our proposed DT system, we present a comparative analysis with recent existing methodologies, as detailed in Table 3. This table highlights the distinctive features of our approach in relation to contemporary methods, thereby facilitating a comprehensive understanding of the respective capabilities of each system. The first column of the table lists the attributes under comparison, which encompass the sensing method, 3D deformation reconstruction, visualization, simulation, interaction with virtual objects, control of real robots, and reconfigurability. The

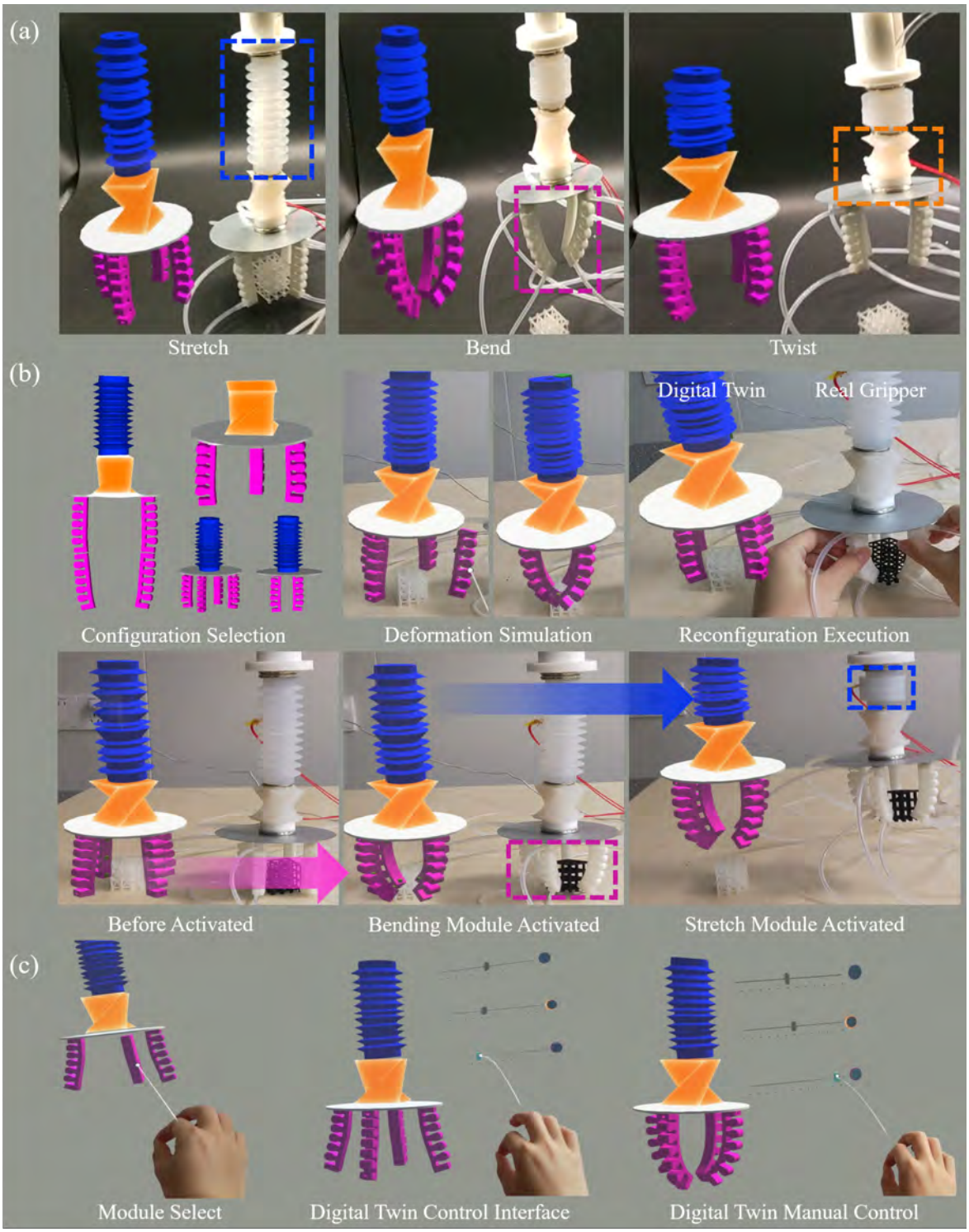

Figure 13: Demonstration for DT system. (a) Visualization patterns for the deformation of three basic modules.(b) Simulation workflow within the DT system (c) AR-enable interactive gestural interface for the human to manipulate the DT, including add/drop modules (left) and simulate the deformation (right).

second column outlines the features of our proposed system, which utilizes strain gauge technology for sensing, enables 3D deformation reconstruction via a skeletal framework, and incorporates AR for visualization. This integration fosters an immersive interaction experience with virtual objects, thereby significantly enhancing user engagement.
In contrast, the analysis revealed that Jin et al.[40] utilized triboelectric nanogenerator sensors; however, their system lacked a mechanism for 3D deformation reconstruction and offered visualization solely through a 2D screen, thus limiting user interaction. Bern et al.[36] employed finite element analysis (FEA) for sensing and delivered a VR visualization experience, yet their approach did not accommodate real-world interaction. Borges et al.[37] similarly utilized a skeletal framework for 3D deformation reconstruction and AR for visualization; however, their system was deficient in simulation and interaction capabilities. Xiang et al.[41] proposed a method that enabled simulation and control of a real robot but lacked several critical aspects, including 3D deformation reconstruction and immersive interactions. Finally, none of the above methods supported multiple deformation types and reconfiguration. The accuracy of 3D geometry reconstruction remains an underexplored area in the literature, with few prior works providing quantitative metrics to evaluate performance. For instance, Jin et al. [40] primarily focus on the accuracy of recognizing different grasped objects rather than quantifying the precision of 3D reconstruction. In contrast, Bern et al. [36] address the accuracy of trajectory tracking in soft robotics. Specifically, they report that the mean absolute error (MAE) of the end effector's position in Cartesian space is 1.8% of the soft robot's length for a circular trajectory, while for user-specified trajectories, the error increases to 2.1% of the robot's length. Borges et al. [37] employ a Feed-Forward Neural Network (FFNN) to predict the 2D points' position of bending soft robots, achieving a mean squared error (MSE) of 0.0094 between the expected results and the neural network outputs. Similarly, Xiang et al. [41] investigate the discrepancy between simulated and real curvature, reporting errors ranging from 0.8% to 3.4%. Notably, both methods observe that the error increases at the higher deformation degree.In our proposed method, we introduce three quantitative metrics in Table.2 to characterize the performance of the three basic soft modules, with errors observed within the range of 0–7.14%. However, it is important to note that these errors are difficult to directly compare with those reported in other studies due to differences in loading conditions, measurement type, and degrees of deformation. Furthermore, the accuracy of our method can be significantly improved through more detailed calibration processes, detailed in Section.3.2.2. This calibration method partially addresses the issue of increasing errors at higher deformation levels, offering a potential pathway for enhanced modeling and control of soft robotic systems.

Our proposed method distinctly stands out by offering immersive AR interaction and comprehensive control mechanisms, thereby signifying a substantial advancement over the examined methodologies, most of which exhibit limitations in one or more domains. In conclusion, the comparative analysis encapsulated in Table.3 elucidates the distinctive advantages of our DT system, thereby positioning it as a robust alternative within the evolving landscape of DT technologies.

Methods	**Ours**	**Jin et al.[40]**	**Bern et al.[36]**	**Borges et al.[37]**	**Xiang et al.[41]**
Sensing Method	Strain gauge	Triboelectric nanogenerator sensors	FEA	Marker and camera	Camera
3D Deformation Reconstruction	Skeleton	None	Skeleton	Skeleton	None
Visualization	AR with 3D geometry	2D screen with 3D geometry	VR with 3D geometry	AR with 3D geometry	2D screen with 3D geometry
Simulation	Enable	None	None	None	Enable
Interaction with Virtual Object	Immersive AR Interaction	None	VR interaction and cannot see the real world	None	None
Control the Real Robot	PID control	Enable	Open loop	None	Enable
Deformation type	Stretch, Bending, Twisting	Bending	Bending	Bending	Bending
Reconfigurability	Enable	None	None	None	None

Table 3: Comparison of various advanced DT methods with ours.

6. Conclusion

This paper introduces a novel framework for developing a DT system for reconfigurable soft robots within an AR setting. The framework involves the integration of armature-based techniques and bending sensors to accurately capture the robots' deformation. The core contributions of this research are delineated as follows:

- The framework employs armature-based techniques to modify and reconstruct the DT corresponding to the soft robot's deformation within the AR milieu, thereby ensuring seamless transitions amongst various 3D deformation states.
- This study delineates three principal deformation patterns, stretching, bending, and twisting, and introduces corresponding visualization patterns that accurately depict these fundamental deformations.
- A sensor fusion approach is deployed to establish a coherent mapping between sensor data and deformation, which significantly enhances the precision of visualization and simulation within the AR framework.
- A platform utilizing AR technology is presented, offering an immersive environment for human engagement with the RSR. This platform introduces human intelligence into the process, optimizing the configuration of the RSR.

- Lastly, the manuscript introduces a PID control strategy aimed at governing the deformation of the soft modules.

In this study, the control of programmable deformation primarily relies on switching air valves, and there is a slight delay in communication between the Arduino and the Hololens. For future development, employing multiple Arduino boards or advanced control boards is advisable, as this would decouple reading and writing operations and improve overall system responsiveness. Regarding the actuation method, the pneumatic approach sometimes exhibits hysteresis, and the speed of shape transformation is dependent on the input pressure; lower pressures can result in slower morphing speeds. Future research may investigate alternative, faster actuation methods, such as electromagnetic actuation, shape memory alloys, or electroactive polymers. These technologies offer the potential for more immediate responses and finer control, which could significantly improve the accuracy and speed of shape-morphing mechanisms. Additionally, advancements in microfluidics or the use of rapid digital valve systems could also provide improvements in the responsiveness of pneumatic systems. Exploring these avenues could lead to more efficient and precise deformable structures suitable for a broader range of applications.

References

[1] N. El-Atab, R. B. Mishra, F. Al-Modaf, L. Joharji, A. A. Alsharif, H. Alamoudi, M. Diaz, N. Qaiser, M. M. Hussain, Soft actuators for soft robotic applications: a review, Advanced Intelligent Systems 2 (2020) 2000128.

[2] A. Brunete, A. Ranganath, S. Segovia, J. P. de Frutos, M. Hernando, E. Gambao, Current trends in reconfigurable modular robots design, International Journal of Advanced Robotic Systems 14 (2017) 1729881417710457.

[3] Z. Liao, J. Chen, Y. Cai, Reconfigurable soft robots based on modular design, Computer-Aided Design & Applications (2023).

[4] J.-Y. Lee, J. Eom, W.-Y. Choi, K.-J. Cho, Soft lego: bottom-up design platform for soft robotics, in: 2018 IEEE/RSJ International Conference on Intelligent Robots and Systems (IROS), IEEE, 2018, pp. 7513–7520.

[5] D. Wang, B. Zhao, X. Li, L. Dong, M. Zhang, J. Zou, G. Gu, Dexterous electrical-driven soft robots with reconfigurable chiral-lattice foot design, Nature Communications 14 (2023) 5067.

[6] C. Freeman, M. Maynard, V. Vikas, Topology and morphology design of spherically reconfigurable homogeneous modular soft robots, Soft Robotics 10 (2023) 52–65.

[7] B. T. Phillips, K. P. Becker, S. Kurumaya, K. C. Galloway, G. Whittredge, D. M. Vogt, C. B. Teeple, M. H. Rosen, V. A. Pieribone, D. F. Gruber, et al., A dexterous, glove-based teleoperable low-power soft robotic arm for delicate deep-sea biological exploration, Scientific reports 8 (2018) 1–9.

[8] Z. Jiao, C. Zhang, W. Wang, M. Pan, H. Yang, J. Zou, Advanced artificial muscle for flexible material-based reconfigurable soft robots, Advanced Science 6 (2019) 1901371.

[9] F. Tao, H. Zhang, A. Liu, A. Y. Nee, Digital twin in industry: State-of-the-art, IEEE Transactions on industrial informatics 15 (2018) 2405–2415.

[10] M. Grieves, J. Vickers, Digital twin: Mitigating unpredictable, undesirable emergent behavior in complex systems, Transdisciplinary perspectives on complex systems: New findings and approaches (2017) 85–113.

[11] E. J. Tuegel, A. R. Ingraffea, T. G. Eason, S. M. Spottswood, Reengineering aircraft structural life prediction using a digital twin, International Journal of Aerospace Engineering 2011 (2011).

[12] B. Wang, H. Zhou, X. Li, G. Yang, P. Zheng, C. Song, Y. Yuan, T. Wuest, H. Yang, L. Wang, Human digital twin in the context of industry 5.0, Robotics and Computer-Integrated Manufacturing 85 (2024) 102626.

[13] F. Tao, B. Xiao, Q. Qi, J. Cheng, P. Ji, Digital twin modeling, Journal of Manufacturing Systems 64 (2022) 372–389.

[14] K. Liu, F. Hacker, C. Daraio, Robotic surfaces with reversible, spatiotemporal control for shape morphing and object manipulation, Science Robotics 6 (2021) eabf5116.

[15] J. Sun, J. Zhao, Physics-based modeling of twisted-and-coiled actuators using cosserat rod theory, IEEE Transactions on Robotics 38 (2021) 779–796.

[16] A. Zhang, R. L. Truby, L. Chin, S. Li, D. Rus, Vision-based sensing for electrically-driven soft actuators, IEEE Robotics and Automation Letters 7 (2022) 11509–11516.

[17] X. Ma, P. W.-Y. Chiu, Z. Li, Shape sensing of flexible manipulators with visual occlusion based on bezier curve, IEEE Sensors Journal 18 (2018) 8133–8142.

[18] R. K. Katzschmann, C. Della Santina, Y. Toshimitsu, A. Bicchi, D. Rus, Dynamic motion control of multi-segment soft robots using piecewise constant curvature matched with an augmented rigid body model, in: 2019 2nd IEEE International Conference on Soft Robotics (RoboSoft), IEEE, 2019, pp. 454–461.

[19] A. Koivikko, V. Lampinen, M. Pihlajamäki, K. Yiannacou, V. Sharma, V. Sariola, Integrated stretchable pneumatic strain gauges for electronics-free soft robots, Communications Engineering 1 (2022) 14.

[20] G. Gerboni, A. Diodato, G. Ciuti, M. Cianchetti, A. Menciassi, Feedback control of soft robot actuators via commercial flex bend sensors, IEEE/ASME Transactions on Mechatronics 22 (2017) 1881–1888.

[21] S. Li, S. A. Awale, K. E. Bacher, T. J. Buchner, C. Della Santina, R. J. Wood, D. Rus, Scaling up soft robotics: A meter-scale, modular, and reconfigurable soft robotic system, Soft Robotics 9 (2022) 324–336.

[22] T. Baaij, M. K. Holkenborg, M. Stölzle, D. Van Der Tuin, J. Naaktgeboren, R. Babuška, C. Della Santina, Learning 3d shape proprioception for continuum soft robots with multiple magnetic sensors, Soft Matter 19 (2023) 44–56.

[23] K. Takaki, Y. Taguchi, S. Nishikawa, R. Niiyama, Y. Kawahara, Acoustic length sensor for soft extensible pneumatic actuators with a frequency characteristics model, IEEE Robotics and Automation Letters 4 (2019) 4292–4297.

[24] Y. Meng, G. Fang, J. Yang, Y. Guo, C. C. Wang, Spring-imu fusion-based proprioception for feedback control of soft manipulators, IEEE/ASME Transactions on Mechatronics (2023).

[25] F. Stella, C. Della Santina, J. Hughes, Soft robot shape estimation with imus leveraging pcc kinematics for drift filtering, IEEE Robotics and Automation Letters (2023).

[26] R. L. Truby, C. Della Santina, D. Rus, Distributed proprioception of 3d configuration in soft, sensorized robots via deep learning, IEEE Robotics and Automation Letters 5 (2020) 3299–3306.

[27] T. G. Thuruthel, B. Shih, C. Laschi, M. T. Tolley, Soft robot perception using embedded soft sensors and recurrent neural networks, Science Robotics 4 (2019) eaav1488.

[28] C. Larson, B. Peele, S. Li, S. Robinson, M. Totaro, L. Beccai, B. Mazzolai, R. Shepherd, Highly stretchable electroluminescent skin for optical signaling and tactile sensing, science 351 (2016) 1071–1074.

[29] R. Zhao, H. Dai, H. Yao, Liquid-metal magnetic soft robot with reprogrammable magnetization and stiffness, IEEE Robotics and Automation Letters 7 (2022) 4535–4541.

[30] H. Zhao, K. O'brien, S. Li, R. F. Shepherd, Optoelectronically innervated soft prosthetic hand via stretchable optical waveguides, Science robotics 1 (2016) eaai7529.

[31] Y. Lu, W. Chen, B. Lu, J. Zhou, Z. Chen, Q. Dou, Y.-H. Liu, Adaptive online learning and robust 3-d shape servoing of continuum and soft robots in unstructured environments, Soft Robotics 11 (2024) 320–337.

[32] Z. Dong, X. Wang, G. Fang, Z. He, J. D.-L. Ho, C.-L. Cheung, W. L. Tang, X. Xie, L. Liang, H.-C. Chang, et al., Shape tracking and feedback control of cardiac catheter using mri-guided robotic platform—validation with pulmonary vein isolation simulator in mri, IEEE Transactions on Robotics 38 (2022) 2781–2798.

[33] T. L. T. Lun, K. Wang, J. D. Ho, K.-H. Lee, K. Y. Sze, K.-W. Kwok, Real-time surface shape sensing for soft and flexible structures using fiber bragg gratings, IEEE Robotics and Automation Letters 4 (2019) 1454–1461.

[34] B. Shih, D. Shah, J. Li, T. G. Thuruthel, Y.-L. Park, F. Iida, Z. Bao, R. Kramer-Bottiglio, M. T. Tolley, Electronic skins and machine learning for intelligent soft robots, Science Robotics 5 (2020) eaaz9239.

[35] R. B. Scharff, G. Fang, Y. Tian, J. Wu, J. M. Geraedts, C. C. Wang, Sensing and reconstruction of 3-d deformation on pneumatic soft robots, IEEE/ASME Transactions on Mechatronics 26 (2021) 1877–1885.

[36] J. M. Bern, W. C. May, A. Osborn, F. Stella, S. Zargarzadeh, J. Hughes, A soft robot inverse kinematics for virtual reality, in: 2024 IEEE International Conference on Robotics and Automation (ICRA), IEEE, 2024, pp. 14957–14963.

[37] E. I. Borges, J. S. Rieder, D. Aschenbrenner, R. B. Scharff, Framework for armature-based 3d shape reconstruction of sensorized soft robots in extended reality, Frontiers in Robotics and AI 9 (2022) 810328.

[38] C. Zhu, Y. Lu, L. Jiang, Y. Yu, Liquid crystal soft actuators and robots toward mixed reality, Advanced Functional Materials 31 (2021) 2009835.

[39] Z. Liao, T. Li, Y. Wang, Y. Cai, Soft pneumatic actuator optimal design based on isogeometric analysis, Manufacturing Letters 35 (2023) 55–63.

[40] T. Jin, Z. Sun, L. Li, Q. Zhang, M. Zhu, Z. Zhang, G. Yuan, T. Chen, Y. Tian, X. Hou, et al., Triboelectric nanogenerator sensors for soft robotics aiming at digital twin applications, Nature communications 11 (2020) 5381.

[41] T. Xiang, B. Li, Q. Zhang, M. Leach, E. Lim, A novel approach to grasping control of soft robotic grippers based on digital twin, in: 2024 29th International Conference on Automation and Computing (ICAC), IEEE, 2024, pp. 1–6.